

Investigating the Influence of Chemical Reaction on MHD-Casson Nanofluid Flow via a Porous Stretching Sheet with Suction/Injection

Damala Chenna Kesavaiah¹, Vellanki Nagaraju², Bhumarapu Venkateswarlu³

¹Department of Basic Sciences & Humanities, Vignan Institute of Technology and Science, Deshmukhi (V), Pochampally (M), Yadadri-Bhuvangiri, Pin: 508284, Telangana, India

²Department of Mathematics, B. V. Raju Institute of Technology, Narsapur-502313, Medak, Telangana, India

³School of Mechanical Engineering, Yeungnam University, Gyeongsan-38541, Republic of Korea

Abstract

This study aims to investigate the influence of chemical reaction on the flow characteristics of a magnetohydrodynamic (MHD) Casson nanofluid over a porous stretching sheet with suction/injection. The nanofluid (NF) is comprised of a base fluid with suspended nanoparticles (NPs), and the Casson fluid (CF) model is employed to capture the non-Newtonian behavior. The governing partial differential equations (PDEs) for momentum, energy, and NP concentration are derived, incorporating the effects of magnetic field, viscous dissipation, chemical reaction, and porous medium. The resulting system of nonlinear ordinary differential equations (ODEs) is solved numerically using the Runge-Kutta-Fehlberg method together with the shooting process. The effects of various physical parameters, such as magnetic field strength, porous medium, CF parameters, NP volume fraction, suction/injection parameter, and chemical reaction parameter, on the flow characteristics are examined in detail. The results reveal that faster movement is linked to higher Grashof numbers and porous mediums, but weaker magnetic fields slow it down. The suction/injection affect velocity inversely. The Prandtl and Eckert numbers have opposite effects on temperature fields. The thermophoresis and Brownian motion parameters affect the opposite trends of the concentration and temperature distributions. The concentration reduces with chemical reaction parameters and the Lewis number. Heat transfer (HT) is enhanced for higher Brownian and thermophoresis. The findings of this study can have potential applications in various engineering fields, such as microfluidics, chemical processing, and thermal management systems, where precise control of fluid flow and heat transfer is essential.

Keywords: *chemical reaction, Casson nanofluid, MHD, porous medium, suction/injection, heat and mass transfer, stretching sheet, viscous dissipation.*

1. Introduction

Investigation into the boundary layer (BL) flow of thick liquids has been the focal point of extensive research by various scientists due to its significance in continuous casting, glass blowing, paper production, polymer expulsion, aerodynamic expulsion of plastic sheets, and other related processes. Sakiadis [1, 2] were the first to study the BL flow over a continuously moving surface. However, many industrial fluids exhibit non-Newtonian behavior. Due to the

complexity of these liquids, there is no single constitutive condition that captures all the properties of such non-Newtonian liquids. One of these non-Newtonian fluid models is known as the Casson fluid (CF), which exhibits yield stress and is characterized as a shear-thinning fluid with infinite viscosity at zero shear rate. The CF is a prominent type of liquid, and its behavior arises from the interactions between the liquid and solid phases. For certain fluids, when the yield stress is significant, it is smaller than the shear stress, and this rheological model performs better than

Corresponding author: Venkateswarlu B (bvenkateswarlu.maths@gmail.com)

Received: 22 March 2023; Revised: 11 July 2023; Accepted: 17 July 2023; Published: 27 July 2023

© 2023 The Author(s). This work is licensed under a Creative Commons Attribution 4.0 International License

the viscoelastic model. Examples of CFs include tomato sauce, jelly, honey, and human blood. Nadeem et al. [3] introduced the 3D CF flow due to an absorbing, linearly extending sheet. Haq et al. [4] studied the convective flow of a Cassonnanoliquid over a contracting sheet influenced by a magnetic field. The CF flow in dual solutions over a stretchable/contracting sheet was investigated by [5]. The authors [6, 7] examined the mass and heat transfer of the MHD CF flow over a penetrable stretching surface. A MHD Casson liquid stream past an oscillating upward plate enclosed in a penetrable medium with a slating wall temperature was examined by Kataria & Patel [8]. Other authors [9-13] have also explored research on Casson nanofluid. Venkateswarlu and Co [14] examine the effects of variable viscosity and viscous dissipation on a porous stretching sheet with hybrid nanofluids and radiative heating. The findings have potential for applications in heating/cooling processes involving temperature-dependent fluid viscosity, like cancer therapy, nanodrug delivery, and power generation.

The study of magnetohydrodynamics (MHD) focuses on the relationship between the electromagnetic field and liquid metals or ferromagnetic particles in a current. It provides insight into the magnetic properties of conductive liquids. The magnetic behavior of NFs has various engineering applications such as MHD sensing and gas pedals, cooling of power generators transmission lines, refrigeration loops, electric transformers, heating elements, dilute liquid problems, cleaning of artificial heart valves, and steam in diverse interaction scenarios. Authors [15, 16] creatively showcased features of 3D radiative magnetized cross fluid via a rotating disk/stretching sheet. Their research discovered that thermophoretic force was boosted, aiding the movement of NPs and leading to a rise in concentration. The MHD Casson NF flow on a 2D surface was examined by Dahab et al. [17]. Nagendra et al. [18] published the article MHD Casson-Carreau fluid flow in a circular horizontal cylinder by using the Keller-Box-Method. In their study, the CF produced better results in comparison to the Carreau fluid. Gopal and Co [19] presented the flow of magneto-Casson NF through an elongated cylinder with slip effects. The

flow of Casson NF over a nonlinear permeable stretched sheet under the influence of a magnetic field and dissipation was investigated by Prabhakar and Shanker [20]. The application of magnetic NF to a constricted artery was demonstrated by Devaki et al. [21]. The erudite scholars [22, 23] delved into the intricate study of the MHD stagnation point flow of radiative micropolar/nanofluid as it interacts with a vertically stretching surface, whilst also taking into account the significant influences of thermophoresis and Brownian motion. Mamun et al. [24] explored the applications of MHD Casson NF particles in various fields such as industries, medicine, the treatment of lung and prostate cancer, etc. Recently, several authors [24-29] have conducted reviews on MHD Casson NFs in different scenarios.

The chemical suspension of NF particles holds great significance in numerous engineering and chemical industry applications. For example, it plays a crucial role in ceramic and polymer production, drying and evaporation processes, food processing, energy transfer in cooling towers, and the flow in desert coolers. A viscosity model for magnetic Carreau fluid characteristics with nanoscale heat transfer and chemical reactions was investigated by Wahab et al. [30, 31]. The fluid is widely used in many fields. The results improve understanding of fluid flow and heat transfer for designing heat exchangers and fluid flow through porous media. Yousef et al. [32] scrutinized the impact of MHD Casson-Williamson NF flow from a chemical perspective. They discovered that in the absence of a magnetic field, NF particles exhibit faster movement. Arulmozhi and coauthors [33] explored the effects of energy and chemical response on magneto NF flow via a moving plate. They noted that the thermal conductivity of copper NF particles is better than that of convectional fluid. Jawad et al. [34, 35] investigate how convective flow affects a Maxwell/Williamson nanofluid Darcy-Forchheimer flow. They examine the effects of thermophoresis, heat conductivity, and chemical reactions using the shot method. The results might help heat transfer devices. Tawade et al. [36] investigated the Brownian motion and chemical response of Casson NF flow by utilizing the shooting method via the R-K process. Goud et al. [37] presented a study on the chemical reaction of the

CF flow over a porous inclined surface, which has practical applications in chemical and magnetic fabric processing. Venkateswarlu and coauthors [38] examined the behavior of CF flow behavior via a porous stretching sheet with thermal conductivity. Several researchers [39-48] have published studies on the chemical impact of MHD Casson NF flow, employing various techniques to obtain solutions.

The aim of this study is to develop a basic assurance model that takes into account the behavior of a CF along with a first-order chemical reaction on a permeable stretching sheet under the influence of suction/injection. In the developed model, various factors such as CF, Brownian motion, thermophoresis, magnetic, permeability, suction/injection, chemical reaction, parameters, and the effects of heat and mass transfer are considered. These parameters play a significant role in understanding the behavior of the fluid and the chemical reactions occurring on the sheet. To analyze the results obtained from the model, a self-comparison is performed. The outcomes are presented in both graphical and tabular forms to facilitate a comprehensive understanding of the system's behavior. The results are qualitatively discussed using a numerical technique called the RKF method. Graphical representations provide a visual depiction of the trends and patterns observed in the system, making it easier to identify significant variations. Furthermore, qualitative discussions help in interpreting the implications of the obtained results.

2. Formulation of the problem

A 2D reliable incompressible progression of a MHD Casson fluid stream induced by a non-straightly stretchable penetrable sheet which is sited at $y = 0$ among synthetically responsive species encountering substance response is considered. Assume that the steam is contemplated about the area and that the initial phase is fixed and the sheet is extended with nonlinear velocity $u_w = ax^n$ in which n is a stretching parameter and x is the arranged estimated alongside the elongating surface $y > 0$. The

coordinates regular with respect to the surface and the fluid streams at $y = 0$.

The liquid is electrically directed because of an applied magnetism $B_0(x)$, which is thought to be common to the expanded sheet. The attractive Reynolds number is accepted, so the actuated magnetic field can be viewed as unimportant. At the extended plane, the wall nanofluid concentration C_w and temperature T_w are thought to be consistent. As $y \rightarrow \infty$, the surrounding estimations of nanofluid concentration and temperature have been indicated by C_∞ and T_∞ correspondingly. The consistent temperature and grouping of the extending surface T_w and C_w are thought to be more prominent than ambient temperature and nanoparticles T_∞ and C_∞ separately.

The anisotropic and Casson fluid flows' rheological articulation can be communicated as (see Ref. [20, 35, 49-50]).

$$\tau_{ij} = \begin{cases} 2 \left(\frac{P_y + \mu_B}{\sqrt{2\pi}} \right) e_{ij}, & \pi > \pi_c \\ 2 \left(\frac{P_y + \mu_B}{\sqrt{2\pi_c}} \right) e_{ij}, & \pi < \pi_c \end{cases} \quad (1)$$

where μ and μ_β are the dynamic and plastic viscosity of non-Newtonian liquid, stress of liquid is p_y , $\pi = e_{ij}e_{ij}$ is the deformation amount of $[i, j]^{th}$ component and π_c is the critical estimations of π .

The concentration, temperature and velocity fields in a steady 2D nanofluid stream are measured as $C = C(x, y), T = T(x, y), v = [u(x, y), v(x, y), 0]$.

From the above suppositions, the conservation equations are designed as (see Ref. [20, 49-50]).

$$\frac{\partial v}{\partial y} + \frac{\partial u}{\partial x} = 0 \quad (2)$$

$$v \frac{\partial u}{\partial y} + u \frac{\partial u}{\partial x} = -\frac{\sigma B_0^2(x)}{\rho_f} u - \frac{v}{K^*} u + v \left(1 + \frac{1}{\beta} \right) \frac{\partial^2 u}{\partial y^2} + g \left[\beta_c (C - C_\infty) + \beta_T (T - T_\infty) \right] \tag{3}$$

$$v \frac{\partial T}{\partial y} + u \frac{\partial T}{\partial x} = \frac{v}{c_\infty} \left(1 + \frac{1}{\beta} \right) \left(\frac{\partial u}{\partial y} \right)^2 + \tau \left\{ D_B \frac{\partial C}{\partial y} \frac{\partial T}{\partial y} + \frac{D_T}{T_\infty} \left(\frac{\partial T}{\partial y} \right)^2 \right\} + \alpha \frac{\partial^2 T}{\partial y^2} \tag{4}$$

$$v \frac{\partial C}{\partial y} + u \frac{\partial C}{\partial x} = \left\{ \frac{D_T}{T_\infty} \left(\frac{\partial^2 T}{\partial y^2} \right) \right\} - Kr^* (C - C_\infty) + D_B \frac{\partial^2 C}{\partial y^2} \tag{5}$$

The boundary conditions for the above flow are

$$y = 0: \begin{cases} v = v_w, & T = T_w, \\ C = C_w, & u_x = ax^n \end{cases} \tag{6}$$

$$y = \infty: \begin{cases} v = 0, T = T_\infty \\ C = C_\infty, & u = 0 \end{cases}$$

Here u & v signifies velocity segments in the x & y -directions, Casson liquid parameter is β , thermal and concentration extension coefficients are β_T & β_C , Brownian dissemination & thermophoresis dispersion coefficient coefficients are D_B & D_T , electrical conductivity is σ , kinematic viscosity is ν , density of the liquid and constituent parts are ρ_f & ρ , g is acceleration due to gravity, K^* is permeability term, Kr^* is chemical response parameter, c is volumetric volume coefficient, and C is rescaled nanoparticles volume portion, thermal diffusivity is $\alpha = \frac{k}{(\rho C)_f}$,

$\tau = \frac{(\rho C)_p}{(\rho C)_f}$ is the proportion of a nanoparticles heat capability along with the base liquid heat capability.

Under the hypothesis to facilitate the uneven magnetic field $B_0(x)$ is of the structure

$$B_0(x) = B_1 x^{\frac{n-1}{2}}.$$

The subsequent non-dimensional parameters are presented as (see Ref. [20, 49-50]).

$$\eta = y \left(\frac{a(n+1)}{2\nu} \right)^{\frac{1}{2}} x^{\frac{n-1}{2}}, \theta(\eta) = \frac{-T + T_w}{-T_w + T_\infty},$$

$$\phi = \frac{-C + C_\infty}{-C_w + C_\infty}, \quad u = ax^n f'(\eta) \tag{7}$$

$$v = - \left(\frac{av(n+1)}{2} \right)^{\frac{1}{2}} x^{\frac{n-1}{2}} \left\{ \begin{array}{l} \frac{(n-1)}{(n+1)} \eta f(\eta) \\ + f(\eta) \end{array} \right\}$$

Assume $v_w = - \left[\frac{av(n+1)}{2} \right]^{\frac{1}{2}} x^{\frac{(n-1)}{2}} S$, where S is the suction parameter.

Equations (2)-(5) along with equation (6) are simplified by adding them to equation (7).

$$f''' \left(1 + \frac{1}{\beta} \right) + ff'' - \left(\frac{\eta f'^2 - G_r \theta}{-G_c \phi} \right) \frac{2}{(n+1)} \tag{8}$$

$$- \left(\frac{1}{K} + M \right) f' = 0$$

$$\left(1 + \frac{1}{\beta} \right) Ec f''^2 + \frac{1}{Pr} \theta'' + Nt \theta'^2 + f \theta' + Nb \phi' \theta' = 0 \tag{9}$$

$$\phi'' + Le f \phi' - Le Kr \phi + \frac{Nt}{Nb} \theta'' = 0 \tag{10}$$

With the boundary situations are

$$\theta(0) = 1, \phi(0) = 1, f(0) = S$$

$$f'(0) = 1, \theta(\infty) = 0, \phi(\infty) = 0 \tag{11}$$

$$f'(\infty) = 0$$

where the prime signifies differentiation according to η . The following physical parameters were used:

Eckert number $E_c = \frac{u_w^2}{C_p (T_w - T_\infty)}$, Grashof and modified Grashof numerals $Gr = \frac{g \beta_T (T_w - T_\infty)}{a^2 x^{2n-1}}$ & $Gc = \frac{g \beta_C (C_w - C_\infty)}{a^2 x^{2n-1}}$, chemical rate parameter $Kr = \frac{Kr^* u (C_w - C_\infty)}{\nu}$, Lewis numeral $Le = \frac{\nu}{D_B}$,

magnetic parameter $M = \frac{2\sigma B_1^2}{a\rho_f(n+1)}$, Brownian motion

parameter $Nb = \frac{D_B(C_w - C_\infty)(\rho C)_p}{v(\rho C)_f}$, thermophoresis parameter

$Nt = \frac{D_T(T_w - T_\infty)(\rho C)_p}{T_\infty v(\rho C)_f}$, Prandtl numeral $Pr = \frac{\nu}{\alpha}$.

3. Solution methodology

The quest for an analytic solution to the boundary value problem (8-11) is a daunting one, for the equations involved are both coupled and highly nonlinear. As such, we must turn to a numerical approach, relying solely on the shooting procedure in conjunction with the RKF technique. To address the problem of solving ordinary differential equations (8)-(10) and their corresponding boundary conditions (11) using the shooting method, we must initially convert these expressions into a series of first-order differential equations.

Assuming that f , θ , and ϕ are represented by z_1, z_4 and z_6 , respectively, i.e.,

$$\left. \begin{aligned} f &= z_1, f' = z_2, f'' = z_3 \\ \theta &= z_4, \theta' = z_5 \\ \phi &= z_6, \phi' = z_7 \end{aligned} \right\} \quad (12)$$

The converted equations are as follows:

$$z_3' = -\left(\frac{1+\beta}{\beta}\right) \left\{ \begin{aligned} z_1 z_3 - \frac{2}{(n+1)} \begin{pmatrix} n z_2^2 \\ -Gr z_4 \end{pmatrix} \\ -\left(\frac{1}{K} + M\right) z_2 \end{aligned} \right\} \quad (13)$$

$$z_5' = -Pr \left\{ \begin{aligned} z_1 z_5 + Nt z_5^2 + Nb z_5 z_7 \\ + \left(1 + \frac{1}{\beta}\right) Ec z_3^2 \end{aligned} \right\} \quad (14)$$

$$z_7' = \left\{ Le z_1 z_7 - Le Kr z_6 + \frac{Nt}{Nb} z_5' \right\} \quad (15)$$

With the BCs are

$$\left. \begin{aligned} z_1(0) = S, z_2(0) = 1, z_4(0) = 1, z_6(0) = 1 \\ z_2(\infty) = 0, z_4(\infty) = 0, z_6(\infty) = 0 \end{aligned} \right\} \quad (16)$$

The quantities of couple stress C_f , Nusselt and Sherwood numerals Nu_x and Sh_x are given as

$$\left. \begin{aligned} C_f &= \frac{\tau_w}{\rho u_w^2}, Nu_x = \frac{xq_w}{k(T_w - T_\infty)}, \\ Sh_x &= \frac{xq_m}{D_B(C_w - C_\infty)} \end{aligned} \right\} \quad (17)$$

Where k signifies thermal conductivity of the nanoliquid, q_w , q_m signifies heat, mass fluxes present at the surface in that order (see Ref. [20, 49-50]) given by

$$\left. \begin{aligned} \tau_w &= \mu_B \left(1 + \frac{1}{\beta}\right) \left(\frac{\partial u}{\partial y}\right)_{y=0} \\ q_w &= -k \left(\frac{\partial T}{\partial y}\right)_{y=0} \\ q_m &= -D_B \left(\frac{\partial C}{\partial y}\right)_{y=0} \end{aligned} \right\} \quad (18)$$

By putting equation (13) into equations (8)-(10), we will get

$$\left. \begin{aligned} Re_x^{\frac{1}{2}} C_f &= \left(1 + \frac{1}{\beta}\right) f''(0), \\ Re_x^{\frac{1}{2}} Nu_x &= -\sqrt{\frac{n+1}{2}} \theta'(0), \\ Re_x^{\frac{1}{2}} Sh_x &= -\sqrt{\frac{n+1}{2}} \phi'(0) \end{aligned} \right\} \quad (19)$$

where $Re_x = \frac{u_w x}{\nu}$ is the Reynolds numeral.

Table 1. The comparison of C_f , Nu and Sh for different variations of β with $Pr = 6.2$, $Ec = 0.5$, $Gr = Gc = 1.0$, $Nb = Nt = 0.2$, $Le = 5.0$, $M = n = 2.0$ and $Kr = 0$, $K = 1/0$.

β	Skin friction (C_f)		Nusselt number (Nu)		Sherwood number (Sh)	
	Previous study [20]	Present study	Previous study [20]	Present study	Previous study [20]	Present study
0.5	1.3702	1.373622	0.3858	0.385764	0.8488	0.848875
1.0	1.7120	1.719122	0.4403	0.440291	0.8578	0.859134
1.5	1.9052	1.905419	0.4602	0.460329	0.8786	0.878587
2.0	2.0233	2.023425	0.4706	0.470775	0.9303	0.930347

4. Validation

Table 1 illustrates the comparison between the preliminary results obtained in the investigation of the friction factor, heat transfer, and mass transfer ratio, and those obtained previously. This comparison reveals a notable level of agreement between the two sets of results [20]. The correlation between the present investigation and the classical works in the field is clear, particularly when compared to the previous study [20], which neglected to consider parameters relating to porous media and chemical reactions. While the current model considers certain parameters such as the magnetic field, thermophoresis diffusion coefficient, Brownian diffusion coefficient, diffusion coefficient, and generation, it excludes those related to porous media and chemical reactions.

5. Results and discussion

The ODEs (8)-(10), as well as the border settings (11) are solved using a shooting technique in R-K-F mode. Brownian motion, magnetic field, permeability, Casson, chemical reaction, thermophoresis parameters, and Lewis, Prandtl, Grashof, and solutal Grashof numbers are used to assess the physical performance of the Casson nanofluid concentration, temperature, and velocity distributions. In addition, the numerical evaluation of Sherwood, Nusselt numbers and the skin friction factor is presented in the tables. For these computations, we use parameter values from a range of values like: $Pr = 6.2$, $Ec = 0.5$, $Le = 5.0$, $Gr = Gc = 1.0$, $K = 0.5$, $Kr = 1.0$, $M = n = 2.0$, and $Nb = Nt = 0.5$.

In Figure 1, the relationship between (a) magnetic field and (b) porous medium intensity velocity plots are depicted. According to Figure 1(a), the liquid velocity decreases as the magnetic intensity rises. These phenomena can be due to the fluid particles being significantly affected by the magnetic field, which acts as a resistance to the liquid's mobility. The charged or magnetizable particles present in a fluid experience forces when a magnetic field is applied to it. These forces may prevent the fluid from moving freely, which would reduce its velocity.

The liquid motion will be more strongly opposed, resulting in a greater drop in velocity, the stronger the magnetic intensity. It is clear from Figure 1(b) that as the permeability of the stretching sheet increases, the velocity also increases. This phenomenon can be understood by considering the behavior of fluid flowing over a stretched surface with pores. As the stretching sheet elongates, the pores on its bounding surface also undergo stretching or elongation. This stretching of the pores significantly affects the flow behavior of the fluid. When the pores are narrow or have a smaller effective cross-sectional area, the fluid encounters restricted space to flow through, resulting in an increase in velocity. In this scenario, the fluid is forced to pass through a smaller area, causing it to accelerate and attain higher velocities. Conversely, as the permeability of the stretching sheet increases, the pores become wider or have a larger effective cross-sectional area. This allows for a greater volume of fluid to pass through the pores, which leads to a higher flow rate but a lower velocity. In other words, the fluid is distributed over a larger area, causing its speed or velocity to decrease.

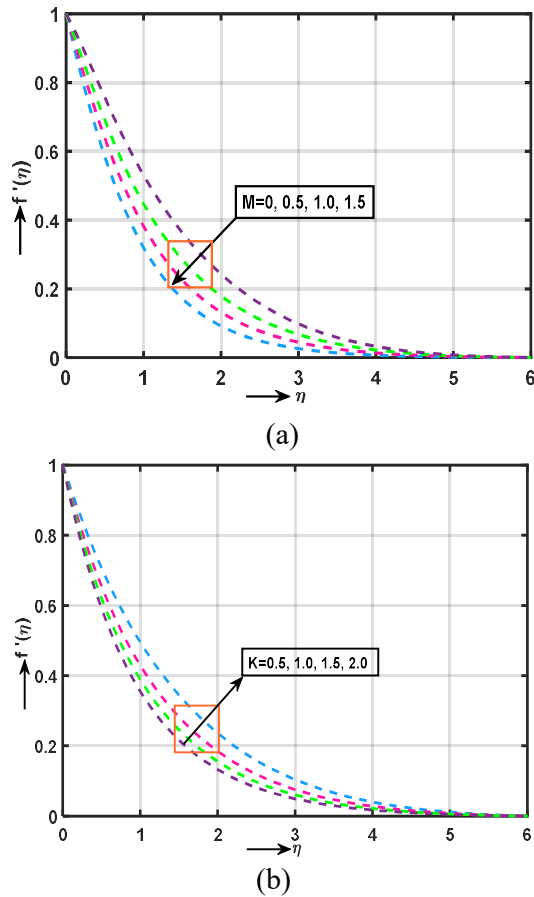


Figure 1. Velocity plots for various estimations of (a) M and (b) K .

The impact of (a) Grashof number (Gr) and (b) modified Grashof numeral (Gm) on the velocity plots is clearly demonstrated in Figure 2. In both cases, it is evident that as these parameters are augmented, the fluid velocity experiences a substantial increase. This phenomenon can be attributed to the fact that both Grashof and modified Grashof numerals have a pronounced effect on fluid viscosity over a larger length scale. Consequently, the fluid expands and dilates, resulting in a notable escalation in velocity. When the Grashof numeral is increased, it directly influences the buoyancy forces acting on the fluid. As a result, the fluid experiences enhanced thermal convection, leading to greater expansion and heightened fluid velocity. Similarly, when the modified Grashof numeral is augmented, it affects the fluid viscosity in a manner that promotes larger-scale fluid expansion and subsequently results in an amplified velocity.

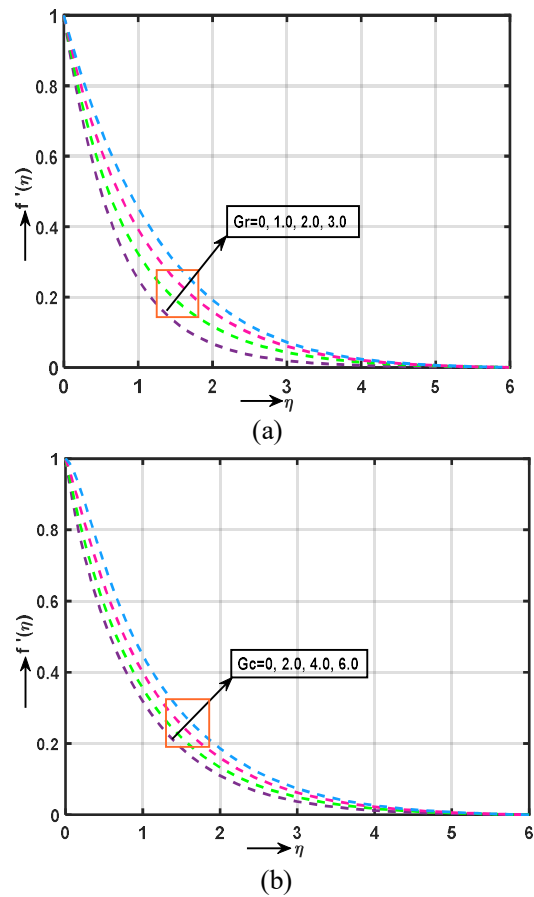


Figure 2. Velocity plots for various estimations of (a) Gr and (b) Gm .

Figure 3 illustrates the impact of the Casson parameter on the (a) velocity and (b) temperature profiles of the fluid. It is evident from the plot that as the Casson parameter increases, the velocity of the fluid decreases. This behaviour can be attributed to the relationship between viscosity and fluid velocity. The β is a characteristic parameter that describes the rheological properties of non-Newtonian fluids, particularly those exhibiting yield stress behaviour. It represents the yield stress and the Casson viscosity, which is the minimum viscosity required for the fluid to flow. When the β is increased, it implies a higher viscosity of the fluid. A higher viscosity signifies greater resistance to flow, which ultimately results in a reduction in fluid velocity. This can be understood by considering the internal friction within the fluid. As the viscosity increases, the fluid experiences greater internal friction, impeding its movement and causing a

decrease in velocity. Furthermore, an increase in viscosity also leads to a decrease in the fluid's ability to deform or flow easily under the influence of external forces. This reduced deformability further contributes to the decrease in fluid velocity as the β rises.

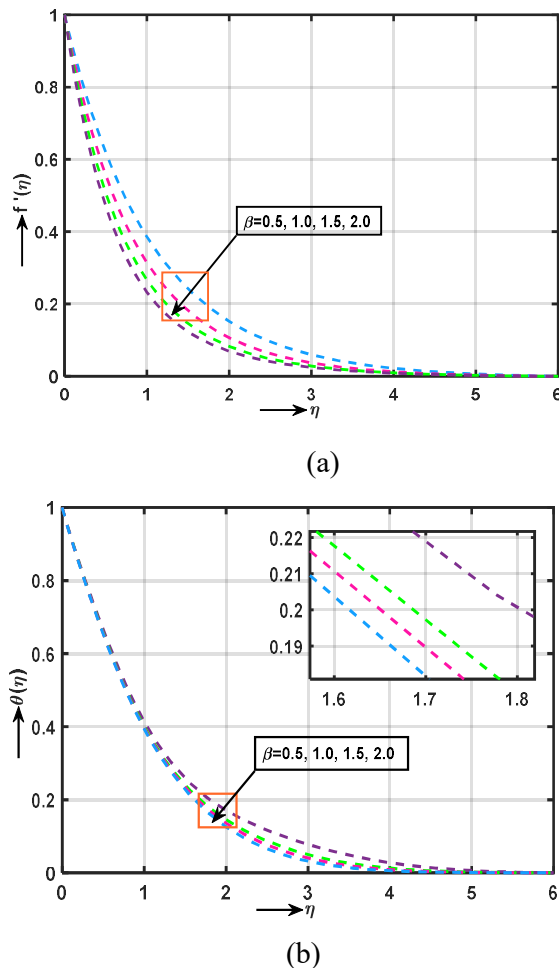


Figure 3. Velocity and temperature plots for various estimations of β

Figure 4 displays the velocity profiles that are influenced by the (a) suction parameter ($S > 0$) and (b) injection parameter ($S < 0$). The suction parameter represents the rate at which fluid is withdrawn from the system. It affects the flow by creating a suction effect, which influences the velocity profiles. When the suction parameter is increased, the velocity of the fluid near the surface decreases. This is because the

suction force acts in the opposite direction of the flow, pulling the fluid away from the surface and reducing its velocity. As a result, the velocity profiles exhibit a decrease in magnitude near the surface as the suction parameter increases. Conversely, the injection parameter represents the rate at which fluid is injected into the system. It has the opposite effect of the suction parameter. As the injection parameter increases, the velocity of the fluid near the surface increases. This is due to the additional fluid being injected into the system, which increases the flow velocity near the surface. Consequently, the velocity profiles exhibit an increase in magnitude near the surface as the injection parameter increases.

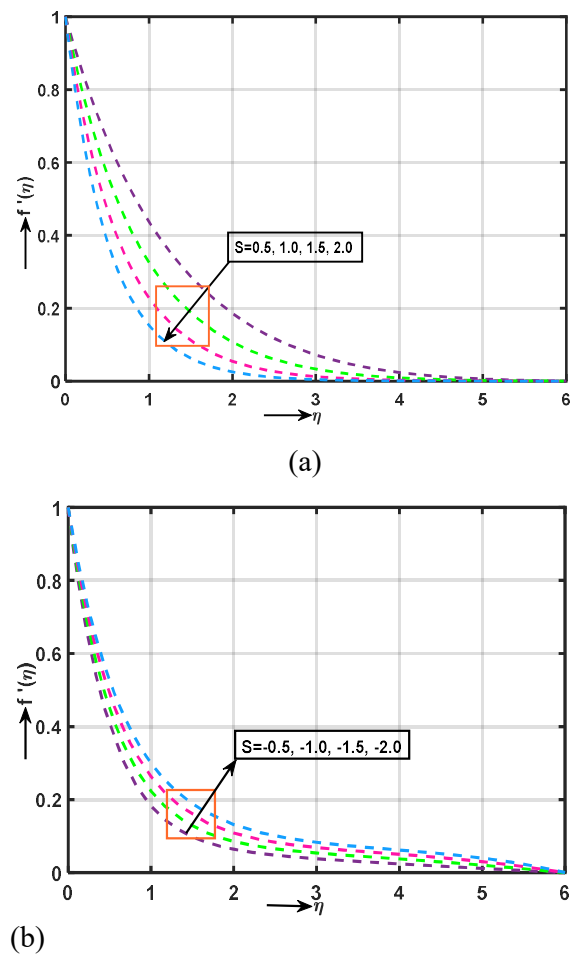


Figure 4. Velocity plots for various estimations of S

The (a) temperature and (b) concentration distributions are depicted in Figure 5 against the

variation of Brownian motion (Nb). It is noticed that the temperature increases when increasing the Brownian motion term because Brownian motion signifies chaotic motion of nanoscale constituent parts in the regular liquid. Consequently, for a large value of Nb , the increment of this chaotic motion gives an increment to the kinetic energy of the nanoscale constituent parts, and therefore, the temperature increases. It is detected that the Brownian motion term elevates the concentration declines due to the nano constituent parts in an irregular way. Hence, this causes a reduction in concentration distribution.

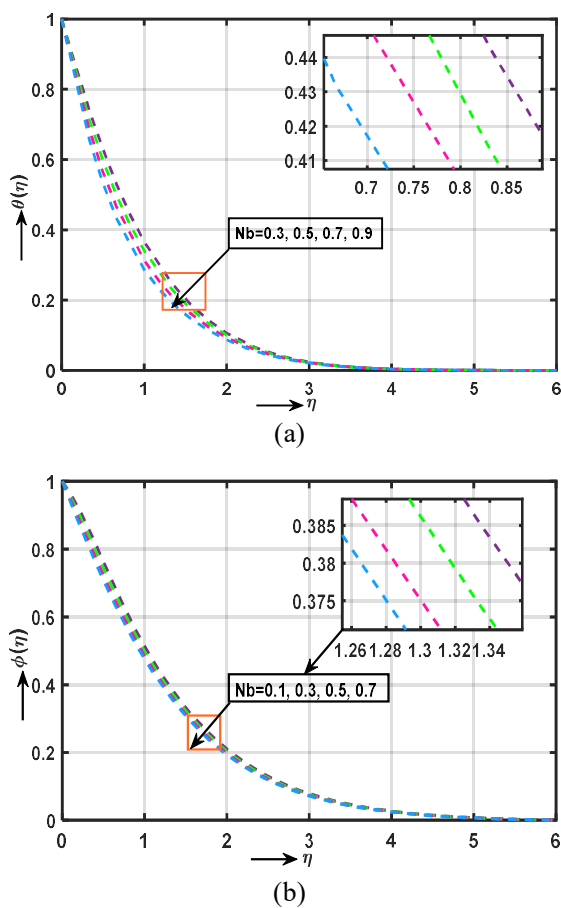


Figure 5. The distributions of (a) temperature and (b) concentration in relation to changes in Nb

Figure 6 demonstrates the influence of the thermophoresis parameter (Nt) on the temperature (a) and concentration (b) profiles individually. The plot clearly indicates that both the temperature and concentration increase as the thermophoresis

parameter is increased. This behavior can be attributed to the phenomenon of thermophoresis, which involves the transport of minor particles away from the warmer region towards the cooler end. Thermophoresis refers to the motion of particles or aerosols in a fluid medium due to temperature gradients. When the thermophoresis parameter is increased, it intensifies the effect of thermophoresis, leading to a more pronounced migration of particles. As a result, the temperature and concentration of these particles increase in the system. The thermophoresis parameter plays a crucial role in modifying the behavior of the thermal boundary layer. By increasing this parameter, the density of the thermal boundary layer also increases. This, in turn, affects the temperature gradient and the rate of mass transfer at the wall surface. As a consequence, the inclination of the temperature and concentration profiles becomes steeper, indicating higher temperatures and concentrations in the fluid.

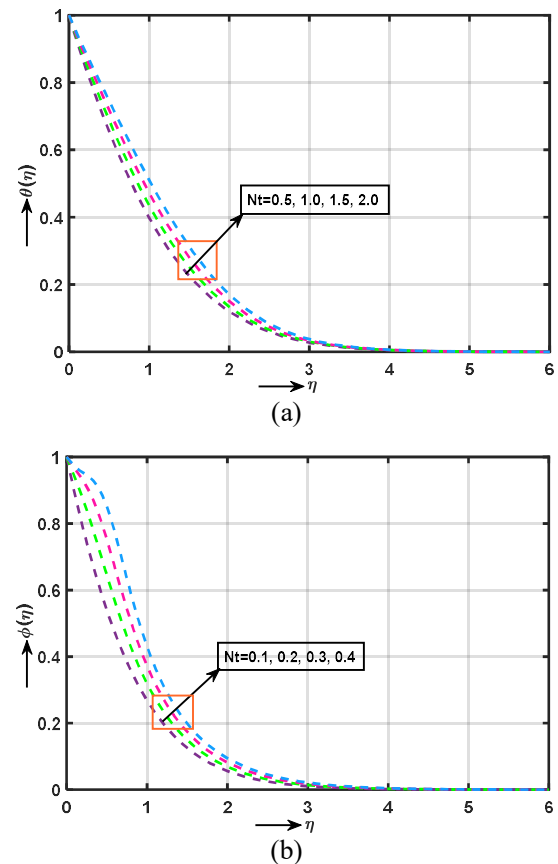


Figure 6. The influence of the Nt on the (a) temperature and (b) concentration profiles.

Figure 7 illustrates the influence of the (a) Prandtl number (Pr) and (b) Eckert number (Ec) on the distribution of temperature.

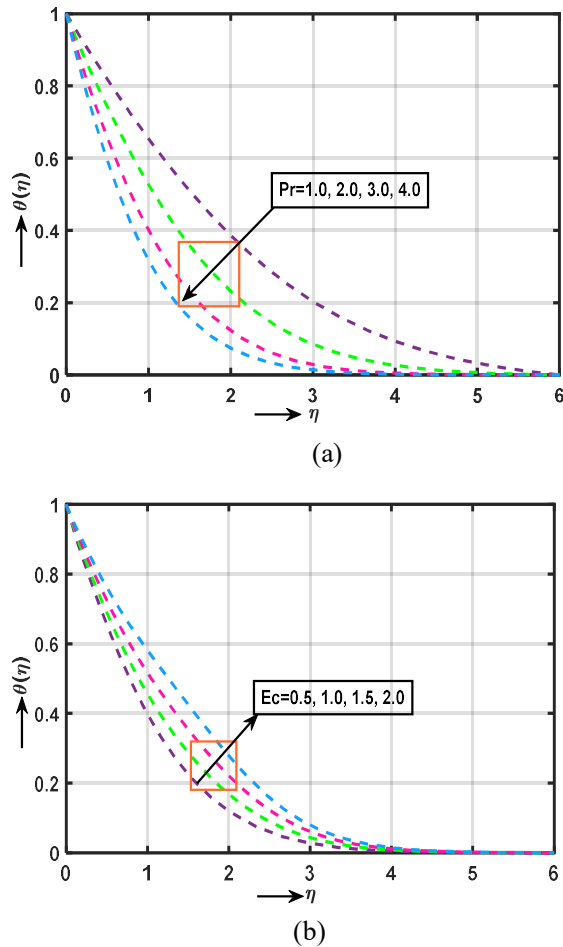


Figure 7. Temperature plots for various estimations of (a) Pr and (b) Ec .

The plot in Figure 7(a) reveals that the Pr has a significant impact on temperature variations. As the Pr increases, the temperature decrease becomes more pronounced. The Pr is a dimensionless parameter that characterizes the ratio of momentum diffusivity to thermal diffusivity in a fluid. It provides insight into the relative magnitudes of these two transport phenomena. When the Pr is higher, it indicates a fluid with lower TC. Consequently, heat dissipates more rapidly from the surface compared to fluids with higher Pr . In other words, fluids with lower Pr possess superior TCs, allowing heat to be rapidly conducted away from the surface. This result in a larger

temperature decreases or drop across the fluid. Moreover, fluids with higher Pr exhibit lower TCs, leading to a slower dissipation of heat and consequently smaller temperature decrements. The Eckert number, on the other hand, influences the rate of cooling for conducting flows. It represents the ratio of kinetic energy to thermal energy in a flow. As the Ec increases, the flow carries more kinetic energy relative to thermal energy, resulting in a faster cooling rate as the fluid temperature rises (Figure 7(b)).

Figure 8 showcases the behavior of the (a) Lewis number (Le) and (b) chemical reaction parameter (Kr) on the concentration profiles.

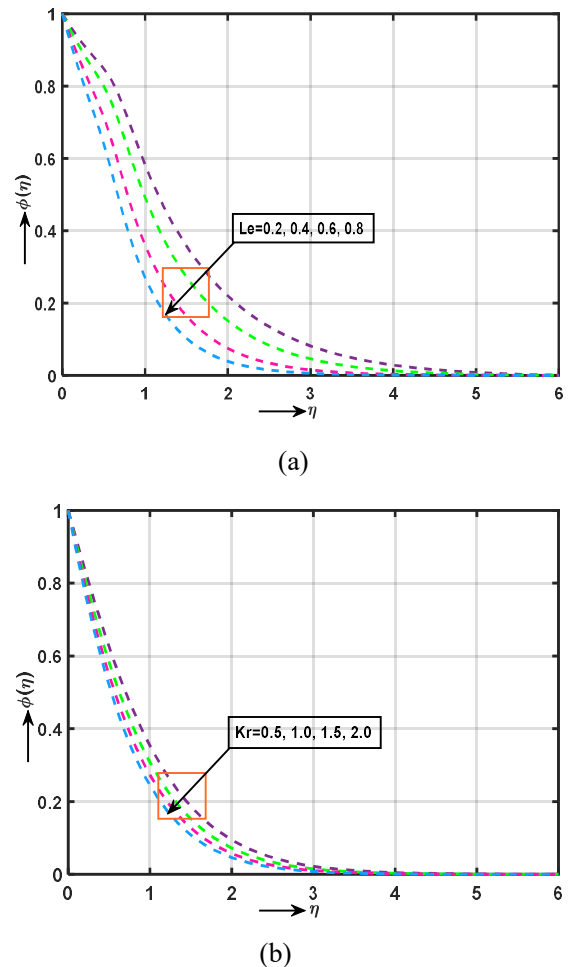


Figure 8. Concentration plots for various estimations of (a) Le and (b) Kr

The plot provides insights into the relationship between these parameters and the concentration of

nanoparticles. Le is a dimensionless parameter that characterizes the ratio of thermal diffusivity to mass diffusivity in a fluid. Figure 8(a) shows that an increase in Le leads to a decrease in NP concentration. This can be attributed to the fact that higher Le indicate greater thermal diffusivity relative to mass diffusivity. As a result, the transport of NPs becomes more influenced by thermal diffusion, causing a reduction in their concentration. Figure 8(b) highlights that larger values of Kr result in a decrease in the concentration of NPs. This observation aligns with the behavior seen in the Le case, where an increase in the chemical reaction parameter leads to a decline in the concentration. The reason behind this trend lies in the fact that as Kr increases, the decay rate of reactant species is enhanced due to the significant influence of the chemical reaction. This, in turn, promotes a higher mass transfer rate, leading to a reduction in the concentration of NPs.

Table A1 and Table A2 present a comprehensive numerical analysis of the variations in skin friction, Nusselt number, and Sherwood number for different parameters. These parameters include the magnetic field, porous medium, Grashof, Prandtl, Schmidt numbers thermophoresis, Brownian motion, Lewis, Eckert numbers, and chemical reaction parameters. The tables provide valuable insights into the effects of these parameters on engineering quantities. The results demonstrate that as these parameters increase, the corresponding engineering quantities also increase. This suggests a positive correlation between the parameters and the studied quantities. However, there are interesting contrasting effects observed in relation to the Prandtl and Eckert numbers on heat transfer rate. These numbers have a different influence on the heat transfer process compared to the other parameters, leading to distinctive trends. The reason behind the observed increments in the engineering quantities with respect to the involved physical parameters can be collectively explained as follows: As the parameters increase, the thermal convective potential of the system rises. This, in turn, leads to an increase in the temperature gradient within the flow domain, particularly between the cold and hot regions. As a result, heat is uplifted and transferred more efficiently.

6. Conclusions

A numerical report was examined for the blended convection MHD stream of Casson nanofluid across a porous extending sheet with gooey dissemination and synthetic response with the assistance of the strategy known as Runge-Kutta-Fehlberg alongside shooting procedure. The parametric report is performed to investigate the impacts of different administering boundaries on the liquid stream, hotness, and mass exchange trademarks. The preliminary results of the study can be summarized as follows:

- The rate of motion experiences an upsurge with greater Grashof numbers and when a porous medium is present, while it dwindles with the amplification of the magnetic field's magnitude.
- The velocity outline displays a reciprocating connection with the suction and injection parameters.
- The thermal and velocity allotments possess contradictory behavior with respect to the Casson parameter.
- When the Prandtl and Eckert numbers increase, the temperature fields behave in an opposite way.
- The temperature and concentration distributions manifest contrary tendencies in relation to the thermophoresis and Brownian motion parameters.
- Both the Lewis number and the conditions of the chemical reaction cause the concentration to decrease.

Abbreviation:

MHD	Magnetohydrodynamic
NF	The nanofluid
NPs	Suspended nanoparticles
CF	Casson fluid
PDEs	Partial differential equations
DEs	Ordinary differential equations
HT	Heat transfer
CF	Casson fluid

Nomenclature

u & v	Velocity component in x, y direction (m/s)
β	Casson liquid parameter
β_T	Brownian dissemination
β_C	thermophoresis
D_B & D_T	Dispersion coefficient coefficients
c	Volumetric volume coefficient
σ	Normal stresses
ν	Kinematic viscosity (m ² /s)
ρ_f & ρ	Density (kg/m ³)
g	Acceleration (m ² /s)
K^*	Permeability (H/m)
Kr^*	chemical response parameter(M/h)
C	rescaled nanoparticles volume portion
τ	Nan particles heat capability
β_0	Magnetic field (kg·s ⁻² ·A ⁻¹)
Sub Scripts	
p	Nano-solid-particles
f	Base fluid

Funding

The authors received no financial support for the research, authorship and publication of this article.

Conflicts of interests/Competing interests

The authors declared no potential conflict of interest with respect to the research, authorship and publication of this article.

Data Availability

The data sharing not applicable to this article as no datasets were generated or analyzed during the current study.

References

- [1] B.C. Sakiadis, "Boundary layer behavior on continuous solid surfaces," *AICHE Journal*, vol. 7, no. 1, pp. 26–28, 1961.
- [2] B.C. Sakiadis, "Boundary layer behavior on continuous solid surfaces: II. Boundary layer on a continuous flat surface," *AICHE Journal*, vol. 7, no. 2, pp. 221–225, 1961.
- [3] S. Nadeem, R. L. Haq, N. S. Akbar and Z. H. Khan, "MHD three-dimensional Casson fluid flow past a porous linearly stretching sheet," *Alexander Engineering Journal*, vol. 52, no. 4, pp. 577–582, 2013.
- [4] R.L. Haq, S. Nadeem, Z.H. Khan and T.G. Okedayo, "Convective heat transfer and MHD effects on Cassonnanofluid flow over a shrinking sheet," *Cent. Eur. J. Phys.*, vol. 12, no. 12, pp. 862–871, 2014.
- [5] P. K. Kameswarani, S. Shaw, P. Sibanda, "Dual solutions of Casson fluid flow over a stretching or shrinking sheet," *Sadhana*, vol. 39, no. 6, pp. 1573–1583, 2014.
- [6] C. K. Kirubhashankar, S. Ganesh, A. M. Ismail, "Casson fluid flow and heat transfer over an unsteady porous stretching surface," *Appl. Math. Sci.*, vol. 9, no. 7, pp. 345–351, 2015
- [7] C. S. K. Raju, N. Sandeep, V. Sugunamma, M. J. Babu, J.V.R. Reddy, "Heat and mass transfer in magnetohydrodynamic Casson fluid over an exponentially permeable stretching surface," *Engineering Science and Technology, an International Journal*, vol. 19, no. 1, pp. 45–52, 2016.
- [8] Kataria H.R., Patel H.R., "Heat and mass transfer in magnetohydrodynamic (MHD) Casson fluid flow past over an oscillating vertical plate embedded in porous medium with ramped wall temperature," *Propulsion and Power Research*, vol. 7, no. 3, pp. 257-267, 2018.
- [9] G. K. Ramesh, G. S. Roopa, A. Rauf, S. A. Shehzad, M. Abbasi, "Time-dependent squeezing flow of Casson-micropolar nanofluid with injection/suction and slip effects," *International Communications in Heat and Mass Transfer*, vol. 126: 105470, 2021.
- [10] I. Zehra, N. Abbas, M. Amjad, S. Nadeem, S. Saleem, A. Issakhov, "Cassonnanofluid flow with Cattaneo-Christov flux analysis over a curved stretching/shrinking channel," *Case Studies in Thermal Engineering*, vol., 27: 101146, 2021.
- [11] J. A. Gbadeyan, E. O. Titiloye, A. T. Adeosun, "Effect of variable thermal conductivity and viscosity on Cassonnanofluid flow with convective heating and velocity slip," *Heliyon*, vol. 6, no. 1: e03076, 2020.
- [12] M. Usman, Z.H. Khan, R. Ahmad, W. Wang, "Dual solutions and stability analysis of flow and heat transfer

- of Casson fluid over a stretching sheet,” *Physics Letters A*, vol. 383, no. 20, pp. 2400–2408, 2019.
- [13] Y. X. Li, M. I. Ur. Rehman, W. H. Huang, M. I. Khan, S. U. Khan, R. Chinram, S. Kadry, “Dynamics of Casson nanoparticles with non-uniform heat source/sink: A numerical analysis,” *Ain Shams Engineering Journal*, vol. 13, no. 1: 101496, 2022.
- [14] B. Venkateswarlu, P. V. S. Narayana, “Cu-Al₂O₃/H₂O hybrid nanofluid flow past a porous stretching sheet due to temperature-dependent viscosity and viscous dissipation,” *Heat Transfer*, vol. 50, no. 1, pp. 432–449, 2020.
- [15] A. Ayub, Z. Sabir, S. Z. H. Shah, H. A. Wahab, R. Sadat, M. R. Ali, “Effects of homogeneous-heterogeneous and Lorentz forces on 3-D radiative magnetized cross nanofluid using two rotating disks,” *International Communications in Heat and Mass Transfer*, vol. 130:105778, 2022.
- [16] H. A. Wahab, S. Z. H. Shah, A. Ayub, Z. Sabir, M. Bila, G. C. Altamirano, “Multiple characteristics of three-dimensional radiative Cross fluid with velocity slip and inclined magnetic field over a stretching sheet,” *Heat Transfer*, vol. 50, no. 4, pp. 3325–3341, 2021.
- [17] S. M. A. Dahab, M.A. Abdelhafez, F. M. Oudina, S.M. Bilal, “MHD Cassonnanofluid flow over nonlinearly heated porous medium in presence of extending surface effect with suction/injection,” *Indian Journal of Physics*, vol. 95, pp. 2703–2717, 2021.
- [18] N. Nagendra, B. Venkateswarlu, Z. Boulahia, CH. Amanulla, G.K. Ramesh, “Magneto-Casson-Carreau fluid flow through a circular porous cylinder with partial slip,” *Journal of Applied and Computational Mechanics*, vol. 50, no. 1, pp. 1–14, 2021.
- [19] D. Gopal, N. Kishan, “Velocity and curvature slip impacts on Cassonnanofluid flow over an inclined magnetic permeable stretching cylinder,” *Journal of Nanofluids*, vol. 8, no. 4, pp. 830–837, 2019.
- [20] B. Prabhakar, B. Shanker, “Mixed convection MHD flow of a Cassonnanofluid over a nonlinear permeable stretching sheet with viscous dissipation,” *Journal of Applied Mathematics and Physics*, vol. 3, pp. 1580–1593, 2015.
- [21] P. Devaki, B. Venkateswarlu, S. Srinivas, S. Sreenadh, “MHD Peristaltic flow of a nanofluid in a constricted artery for different shapes of nanosized particles,” *Nonlinear Engineering*, vol. 9, no. 1, pp. 51–59, 2019.
- [22] M. Jawad, K. S. Nisar, “Upper-convected flow of Maxwell fluid near stagnation point through porous surface using Cattaneo-Christov heat flux model,” *Case Studies in Thermal Engineering*, vol. 48: 103155, 2023.
- [23] R. Safdar, M. Jawad, S. Hussain, M. Imran, A. Akgül, W. Jamshed, “Thermal radiative mixed convection flow of MHD Maxwell nanofluid: Implementation of buongiorno's model,” *Chinese Journal of Physics*, vol. 77, pp. 1465–1478, 2022.
- [24] N. S. Yousef, A. M. Megahed, N. I. Ghoneim, M. Elasfi, E. Fares, “Chemical reaction impact on MHD dissipative Casson–Williamson nanofluid flow over a slippery stretching sheet through porous medium,” *Alexandria Engineering Journal*, vol. 61, no. 12, pp. 10161–10170, 2022.
- [25] H. B. Lanjwani, M. S. Chandio, M. I. Anwar, S. A. Shehzed, M. Izadi, “MHD laminar boundary layer flow of radiative Fe-Cassonnanofluid: Stability analysis of dual solutions,” *Chinese Journal of Physics*, vol. 76, pp. 172–186, 2022.
- [26] W. N. N. Noranuar, A. Q. Mohamad, S. Shafie, I. Khan, L. Y. Jiann, M. R. Ilias, “Non-coaxial rotation flow of MHD Cassonnanofluid carbon nanotubes past a moving disk with porosity effect,” *Ain Shams Engineering Journal*, vol. 12, no. 4, pp. 4099–4110, 2021.
- [27] G. Rasool, A. J. Chamkha, T. Muhammad, A. Shafiq, I. Khan, “Darcy-Forchheimer relation in Casson type MHD nanofluid flow over non-linear stretching surface,” *Propulsion and Power Research*, vol. 9, no. 2, pp. 159–168, 2020.
- [28] A. Kamran, S. Hussain, M. Sagheer, N. Akmal, “A numerical study of magnetohydrodynamics flow in Cassonnanofluid combined with Joule heating and slip boundary conditions,” *Results in Physics*, vol. 7, pp. 3037–3048, 2017.
- [29] F. A. Alwawi, H. T. Alkassabeh, A. M. Rashad, R. Idris, “MHD natural convection of sodium alginate Cassonnanofluid over a solid sphere,” *Results in Physics*, vol. 16: 102818, 2020.
- [30] H.A. Wahab, S.Z.H. Shah, A. Ayub, Z. Sabir, R. Sadat, M. R. Ali, “Heterogeneous/homogeneous and inclined magnetic aspect of infinite shear rate viscosity model of Carreau fluid with nanoscale heat transport,” *Arabian Journal of Chemistry*, vol. 16, no. 5, 2023.
- [31] M. Jawad, M. Muti-Ur-Rehman, K. S. Nisar, “Bioconvection Effects on non-Newtonian chemically reacting Williamson nanofluid flow due to stretched sheet with heat and mass transfer,” *East European Journal of Physics*, pp. 359–369, 2023.
- [32] N. S. Yousef, A. M. Megahed, N. I. Ghoneim, M. Elsaifi, E. Fares, “Chemical reaction impact on MHD dissipative Casson-Williamson nanofluid flow over a slippery stretching sheet through porous medium,” *Alexandria Engineering Journal*, vol. 61, no. 12, pp. 10161–10170, 2022.
- [33] S. Arulmozhi, K. Sukkiramathi, S. S. Santra, R. Edwan, U. F. Gamiz, S. Noeiaghdam, “Heat and mass transfer analysis of radiative and chemical reactive effects on

- MHD nanofluid over an infinite moving plate,” *Results in Engineering*, vol. 14:100394, 2022
- [34] M. Jawad, M. K. Hameed, K. S. Nisar, A. H. Majeed, “Darcy-Forchheimer flow of maxwell nanofluid flow over a porous stretching sheet with Arrhenius activation energy and nield boundary conditions,” *Case Studies in Thermal Engineering*, vol. 44: 102830, 2023.
- [35] J. V. Tawade, C. N. Guled, S. Noeiaghdam, U. F. Gamiz, V. Govindan, S. Balamuralitharan, “Effects of thermophoresis and Brownian motion for thermal and chemically reacting Casson nanofluid flow over a linearly stretching sheet,” *Results in Engineering*, vol. 15:100448, 2022.
- [36] B. S. Goud, Y. D. Reddy, W. Jamshed, K. S. Nisar, A. N. Alharbi, R. Chouikh, “Radiation effect on MHD Casson fluid flow over an inclined non-linear surface with chemical reaction in a Forchheimer porous medium,” *Alexandria Engineering Journal*, vol. 61, no. 10, pp. 8207–8220, 2022.
- [37] B. Venkateswarlu, P. V. S. Narayana, “Influence of variable thermal conductivity on MHD Casson fluid flow over a stretching sheet with viscous dissipation, Soret and Dufour effects,” *Frontiers in Heat and Mass Transfer*, vol. 7, no. 1, pp. 1–9, 2016.
- [38] B. Venkateswarlu, P. V. S. Narayana, “Chemical reaction and radiation absorption effects on the flow and heat transfer of a nanofluid in a rotating system,” *Applied Nanoscience*, vol. 5, no. 3, pp. 351–360, 2015.
- [39] B. Venkateswarlu, P. V. S. Narayana, “Variable wall concentration and slip effects on MHD nanofluid flow past a porous vertical plate,” *Journal of Nanofluids*, vol. 8, no. 4, pp. 838–844, 2019.
- [40] A. Zaib, M. M. Rashidi, A. J. Chamkha, K. Bhattacharyya, “Numerical solution of second law analysis for MHD Casson nanofluid past a wedge with activation energy and binary chemical reaction,” *International Journal of Numerical Methods for Heat & Fluid Flow*, vol. 27, no. 12, pp. 2816–2834, 2017.
- [41] G. R. Ganesh, W. Sridhar, “MHD radiative Casson-nanofluid stream above a non-linear extending surface including chemical reaction through Darcy-Forchheimer medium,” *Heat Transfer*, vol. 50, no. 8, pp. 7691-7711, 2021.
- [42] N. A. M. Noor, S. Shafie, M. A. Admon, “MHD squeezing flow of Casson nanofluid with chemical reaction, thermal radiation and heat generation/absorption,” *Journal of Advanced Research in Fluid Mechanics and Thermal Sciences*, vol. 68, no. 2, pp. 94–111, 2020.
- [43] G. Narender, K. Govardhan, G. S. Sarma, “MHD Casson nanofluid past a stretching sheet with the effects of viscous dissipation, chemical reaction and heat source/sink,” *Journal of Applied Computational Mechanics*, vol. 7, no. 4, pp. 2040–2048, 2021.
- [44] MD. Shamsuddin, S. R. Mishra, T. Thumma, “Chemically reacting radiative Casson fluid over an inclined porous plate: a numerical study,” *Numerical Heat Transfer and Fluid Flow*, pp. 469–479, 2019.
- [45] S. M. Ibrahim, G. Lorenzini, P. V. Kumar, C. S. K. Raju, “Influence of chemical reaction and heat source on dissipative MHD mixed convection flow of a Casson nanofluid over a nonlinear permeable stretching sheet,” *International Journal of Heat and Mass Transfer*, vol. 111, pp. 346–355, 2017.
- [46] I. Ullah, S. Shafie, O. D. Makinde, I. Khan, “Unsteady MHD flanker-Skan flow of Casson nanofluid with generative/destructive chemical reaction,” *Chemical Engineering Science*, vol. 172, pp. 694–706, 2017.
- [47] H. R. Kataria, H. R. Patel, “Radiation and chemical reaction effects on MHD Casson fluid flow past an oscillating vertical plate embedded in porous medium,” *Alexandria Engineering Journal*, vol. 55, no. 1, pp. 583–595, 2016.
- [48] S. A. Shehzad, T. Hayat, M. Qasim, S. Asghar, “Effects of mass transfer on MHD flow of Casson fluid with chemical reaction and suction,” *Brazilian Journal of Chemical Engineering*, vol. 30, pp. 187–195, 2013.
- [49] P. Rana, R. Bhargava, “Flow and heat transfer of a nanofluid over a nonlinearly stretching sheet: A Numerical study,” *Communications in Nonlinear Science and Numerical Simulation*, vol. 17, pp. 212–226, 2012.
- [50] F. Mabood, W. A. Khan, A. I. M. Ismail, “MHD boundary layer flow and heat transfer of nanofluids over a nonlinear stretching sheet: A Numerical study,” *Journal of Magnetism and Magnetic Materials*, vol. 374, pp. 569–576, 2015.

Appendix

Table A1. Numerical calculations of C_f , Nu and Sh for dissimilar variations of parameters.

M	K	Gr	Gc	Pr	Sc	C_f	Nu	Sh
1.0	0.5	0.5	0.5	0.71	0.5	1.51604	1.63889	0.20488
2.0						1.73129	1.99526	0.56020
3.0						1.92073	2.38577	0.94932
4.0						2.09169	2.82122	1.38318
2.0	0.5					1.60769	0.46039	0.77151
	1.0					1.64363	0.51979	0.78215
	1.5					1.71318	0.54145	0.80271
	2.0					1.90549	0.55268	0.85914
		0.0				1.64651	0.46039	0.77026
		0.5				1.73146	0.49395	0.79789
		1.0				1.81764	0.52536	0.82745
		1.5				1.90549	0.55442	0.85914
			0.2			1.61020	0.46039	0.74170
			0.4			1.70913	0.50424	0.77906
			0.5			1.80765	0.54616	0.81811
			2.0			1.90549	0.58599	0.85914
				0.71		1.90105	0.11428	1.12788
				1.0		1.90338	0.15737	1.19019
				3.0		1.90883	- 0.38586	1.73420
				7.0		1.91028	- 1.47163	2.83249
					0.5	1.90105	1.09951	1.12788
					1.0	1.91322	1.10900	1.49228
					1.5	1.92068	1.12508	1.74979
					2.0	1.925841	1.15737	1.95669

Table A2. Numerical calculations of C_f , Nu and Sh for dissimilar variations of parameters.

Nb	Nt	Le	Kr	Ec	C_f	Nu	Sh
1.0	0.2	0.5	0.5	0.3	1.896521	- 0.045281	1.010039
2.0					1.901798	0.073887	1.018814
3.0					1.907726	- 0.118155	1.021128
4.0					1.913324	0.254062	1.021326
	0.2				1.903635	0.179861	1.010039
	0.4				1.906550	0.203446	1.028036
	0.6				1.909776	0.228163	1.054111
	0.8				1.913324	0.254062	1.087594
		0.2			1.895012	0.141250	0.952805
		0.4			1.898996	0.151687	1.066423
		0.6			1.903062	0.163298	1.192170
		0.8			1.907113	0.175852	1.328702
			0.5		1.901025	0.099501	1.127858
			1.0		1.913282	0.109090	1.492278
			1.5		1.920658	0.125098	1.749789
			2.0		1.925841	0.157357	1.956639
				0.5	1.896805	0.066376	1.214831
				1.0	1.897858	- 0.206602	1.475794
				1.5	1.898912	- 0.388591	1.649783
				2.0	1.900496	- 0.570584	1.823786